Numerical and Experimental Investigation of Phaseless Spherical Near-Field Antenna Measurements

Fernando Rodríguez Varela, Javier Fernandez Álvarez, Belén Galocha Iragüen, Manuel Sierra Castañer, *Senior Member, IEEE*, and Olav Breinbjerg, *Fellow, IEEE*

***Abstract*— This article presents a thorough study of spherical probe-corrected phaseless near-field measurements with the two-scans technique. Such technique is based on retrieving the antenna under test radiation pattern from the measurement of the near-field amplitude signals on two spheres of different radii. The postprocessing of this type of measurements results in a highly nonlinear algorithm, prone to get trapped in local minima and provide incorrect solutions when the measurement conditions are not properly selected. Through a series of numerical simulations, the influence of different measurement parameters on the phaseless technique is analyzed. It will be shown how both the relative and absolute values of the measurement spheres highly affect the convergence of the phase retrieval algorithm. The type of AUT and its radiation pattern characteristic also play a fundamental role in the feasibility of phaseless measurements. Other parameters such as sampling rate, noise, probe correction, polar truncation, and measurement offsets are also investigated. The conducted study allows to extract a set of guidelines to improve the accuracy of phaseless spherical near-field algorithms. In addition, purely phaseless antenna measurement examples are given to demonstrate the algorithm capabilities and limitations, and to validate the developed numerical investigations.**

***Index Terms*— Amplitude-only, antenna measurements, phase retrieval, phaseless measurement, spherical wave expansion.**

I. Introduction

SPHERICAL near-field measurements [1]–[3] are a well-stablished technique for antenna testing. Scanning the field radiated by an antenna under test (AUT) on a spherical surface, followed by efficient postprocessing techniques, leads to the determination of the radiation pattern. For a successful far-field transformation, an accurate amplitude and phase characterization of the AUT near-field is required. Obtaining a stable phase reference can be impractical or even unfeasible, especially at high frequencies, due to inaccuracies of measurement equipment or probe positioning, cable bending and thermal drift, among others. On the other hand, the field magnitude possesses a higher robustness against these factors, leading to the rise of "phaseless" or "amplitude-only" measurement techniques [4].

The improved robustness of amplitude measurements comes with the price of providing very limited information about AUT radiation pattern. Therefore, the lack of phase must be compensated by other means, resulting in different phaseless techniques which rely on extra hardware such as interferometry circuits [5], [6] and holography [7], or multiple scan surfaces [8]. The common objective of such approaches is to measure only the amplitude field in different radiation conditions, so enough independent signals are acquired to extrapolate the phase. An excellent study of state-of-the-art phase retrieval methods is provided in [9]. A major conclusion drawn from it is that the phase retrieval constitutes a non-linear and non-convex mathematical problem, which makes it prone to get trapped in local minima or false solutions. The only way of avoiding local minima is the use of advanced optimization techniques [10] and adding measurement redundancy (oversampling [11], multiple surfaces [12], partial knowledge of phase [13], field spatial derivatives [14], different probes [15]).

From the different phaseless techniques, those based on multiple scan surfaces constitute an attractive alternative because they can be implemented in traditional measurement setups without any hardware modification. This led to the development of the two-scans planar [16]–[19] and spherical [20]–[22] techniques, in which the AUT radiation pattern is extrapolated from the measurement of near-field intensities over two planes or two spheres, respectively.

The two-scans planar technique has been thoroughly studied by different authors, showing a high dependence on the availability of a phase initial guess for a successful transformation [17]. In some cases, the classical plane wave spectrum formulation [23], commonly used to address the processing of the planar near-fields, is replaced by equivalent current approaches solved with method of moments [24], [25]. Even though the computational efficiency is reduced, enforcing unknown currents over the antenna aperture or shape brings additional information to the phase retrieval problem.

Manuscript received November 24, 2020; revised May 8, 2021; accepted May 29, 2021. Date of publication June 25, 2021; date of current version December 16, 2021. This work was supported in part by the Universidad Politécnica de Madrid (Programa Propio) and in part by the Spanish Government, Ministry of Economy, National Program of Research, Development and Innovation through the Project FUTURE-RADIO Radio Systems and Technologies for High Capacity Terrestrial and Satellite Communications in a Hyperconnected World under Grant TEC2017-85529-C3-1-R. *(Corresponding author: Fernando Rodríguez Varela.)*

Fernando Rodríguez Varela, Belén Galocha Iragüen, and Manuel Sierra Castañer are with the Information Processing and Telecommunications Center, Radiation Group, Department of Signals, Systems and Radiocommunications, ETSI Telecomunicación, Universidad Politécnica de Madrid, 28040 Madrid, Spain (e-mail: f.rodriguezv@upm.es).

Javier Fernandez Álvarez is with the Technical University of Denmark, 2800 Kongens Lyngby, Denmark (e-mail: jafealv@elektro.dtu.dk).

Olav Breinbjerg was with the Technical University of Denmark, 2800 Kongens Lyngby, Denmark. He resides in Copenhagen, Denmark (e-mail: olavbreinbjerg@outlook.com).

Color versions of one or more figures in this article are available at https://doi.org/10.1109/TAP.2021.3090846.

Digital Object Identifier 10.1109/TAP.2021.3090846

The use of equivalent currents can be extended to arbitrary scanning geometries, including cylindrical [26] and spherical [9] surfaces. In the latter case, however, the use of spherical wave expansion (SWE) [3] as a field expansion basis becomes appealing with several advantages over the equivalent current approaches. First, an improved computational complexity becomes evident with the use of heavily optimized fast Fourier transform techniques for the processing of fields. Secondly, the SWE constitutes a compact basis representing all degrees of freedom of the AUT field, keeping the number of unknowns to the minimum. Finally, no *a priori* knowledge about the AUT is required apart from its minimum sphere.

In this sense, the two-scans spherical technique has been comparatively less studied, but it has been applied to sophisticated antennas showing low transformation errors and promising capabilities [21]. Parametric studies report that the difference between measurement sphere radii in terms of wavelength is the key for a good phase retrieval convergence. However, it is expected that other parameters like the antenna dimension and its radiation pattern will have a significant influence. Given the nonlinear nature of the problem, such study becomes a critical tool to assess the conditions required for a successful far-field transformation of a given AUT.

This article presents a continuation of the work introduced in [21], by performing a thorough analysis of the two-scans spherical phaseless technique. On Section II, a theoretical background is given to revisit the two-scans phaseless iterative algorithm formulation. In Section III, the influence of the spheres measurement radii, AUT electrical dimensions and type, sampling rate, truncation, probe radiation pattern, and noise are studied by means of simulation antenna models. The derived analysis can be used to design the phaseless measurement conditions for an arbitrary antenna. This will be demonstrated in Section IV with the application of the phase retrieval algorithm to measurements performed in anechoic chamber. Section V concludes this article.

II. Theoretical Background

Considered it is a spherical near-field measurement scenario with an AUT placed at the coordinate system origin. The field radiated by the AUT is measured by a single-order probe in the coordinates (r, θ, φ) pointing to the origin and with a rotation angle χ respect to $\hat{\theta}$. Under such circumstances, the signal measured by the probe is given by the well-known transmission formula [3]

$$w(r, \chi, \theta, \varphi) = \sum_{smn\mu} Q_{smn} e^{jm\varphi} d^n_{\mu m}(\theta) e^{j\mu\chi} P_{s\mu n}(r) \qquad (1)$$

being Q_{smn} the AUT Spherical Wave Coefficients (SWC), $d^n_{\mu m}(\theta)$ a rotation operator, and $P_{s\mu n}(r)$ the probe response constants. The summation in (1) spans for $s \in [1, 2], n \in [1, N]$, $m \in [-n, n]$, and $\mu \in [-1, 1]$. N is the expansion truncation number given by the following rule of thumb for 8-digit accuracy [27]:

$$N = \lceil kr_0 \rceil + 10 \qquad (2)$$

where k is the wavenumber, r_0 the radius of the smallest sphere circumscribing the AUT and the brackets indicate the largest integer smaller than or equal to the number inside them.

If w is sampled on an equiangular grid for two orthogonal polarizations, an algorithm exists [3] for obtaining Q_{smn} with the same computational complexity than that of summation (1): $O(N^3)$. Once these coefficients are known they can be inserted back in (1) to compute the field at any other distance, including the far-field.

When only the amplitude of the probe signal is acquired, a phase retrieval algorithm must be used. Several techniques have been proposed for different applications and antenna measurement configurations. For phaseless spherical near-field measurements, iterative Fourier techniques have been proposed [20], [21] analogous to the ones used in phaseless planar measurements. These techniques are based on the fine-up [28] reduction method, a generalization of the Gerchberg-Saxton algorithm [29] that can be used in any problem in which partial constraints are known in each of two domains. These domains are usually the object to be measured and its Fourier transform, while the constraints are given in terms of amplitude measurements or *a priori* information. The complex information from the object is retrieved by transforming back and forth between the two domains and satisfying the constraints in one before returning to the other.

In phaseless spherical measurements, the two domains correspond to the near-field on each of the measurement spheres, and the constraints are given by the magnitude information of the fields. The magnitudes are denoted by $w_1 = |w(r_1)|$ and $w_2 = |w(r_2)|$, while the spherical surfaces are S_1 and S_2. Note that w_1 and w_2 both contain the measured near-field for two probe orthogonal orientations. Optionally an initial phase guess can be added to the first measurement to generate a complex field $w_1 = |w(r_1)|e^{-j\Phi 1}$. Then, an iterative algorithm is started:

1) w_1 is propagated from S_1 to S_2 by means of the SWE formulation, obtaining a new calculated complex field, $\tilde{w}_2 = |\tilde{w}_2|e^{-j\Phi 2}$;
2) $\tilde{w}_2$ is compared to the measured magnitude w_2 by a certain near-field error metric;
3) $|\tilde{w}_2|$ is discarded and substituted by w_2, resulting in complex field $\tilde{w}'_2 = w_2 e^{-j\Phi 2}$;
4) $\tilde{w}'_2$ is then propagated back to S_1 and the analogous amplitude substitution is performed.

This iterative process of propagation and magnitude substitution is continued after the error metric drops below a given threshold or a specified number of iterations is reached.

Two error metrics will be used along this article. The first one is the amplitude error, and is the one that can be used in the iterative algorithm as a stopping criterion

$$\varepsilon_{amp} = \frac{rms(|\tilde{w}_2| - w_2)}{max(w_2)} \qquad (3)$$

where rms denotes the computation of the root mean square error over all angular points of the measured field. In addition, a complex error metric will be defined too

$$\varepsilon_{comp} = \frac{rms\left(Q_{smn} - \tilde{Q}_{smn}\right)}{max(Q_{smn})} \qquad (4)$$

where $\tilde{Q}_{smn}$ denotes the retrieved SWC of the AUT at a given iteration of the iterative algorithm and Q_{smn} are the true coefficients. Of course, this metric can only be computed when the SWC of the AUT are *a priori* known, so it is not applicable on a real phaseless measurement scenario. However, it will be used to assess the performance of the phase retrieval technique in different experiments through this article.

III. Numerical Discussion

On this section, the two-scans spherical phaseless technique is tested using a simulation model based on dipole antennas [30]. By arranging electric and magnetic dipoles in array configurations, different AUTs of arbitrary size can be simulated using analytical formulation to emulate aperture antennas. The same principle may be applied for designing probes with the desired directivity. The flexibility of this model will be exploited to analyze the influence of different parameters of the measurement setup over the performance of the phase retrieval technique. For convenience, the AUTs will be simulated as planar arrays of equi-spaced Huygens sources (crossed magnetic and electric dipoles) with horizontal polarization. The Huygens sources produce a unidirectional pattern canceling the back radiation. Separation between Huygens sources is set to 0.1λ forming a uniform grid, while the number of them and its amplitude and phase distribution will be adjusted according to the different experiments. Therefore, the AUT pattern is adjusted by controlling the array factor weights and the number of individual sources. To refer to the size of such arrays, the truncation number N corresponding to its minimum sphere will be used. All measurement radii will be normalized to the Rayleigh far-field distance of each AUT: $r_{far} = 2\frac{(2r_0)^2}{\lambda}$.

In every experiment presented in this section, a near-field measurement will be simulated in an equiangular grid of increments $\Delta\varphi = \Delta\theta = \frac{\pi}{sN}$, being s an angular oversampling ratio, greater than or equal to 1. This oversampling ratio is defined so that $s = 1$ corresponds to the sampling rate of standard spherical near-field measurements [3]. For each measurement point two orthogonal polarizations are measured. The measured field is simulated on two spheres of radii r_1 and r_2, and the proposed phase retrieval technique is applied for 1000 iterations using amplitude-only information. In all simulations, the initial guess will be the phase of an Hertzian dipole with the same polarization as of the AUT. Finally, the accuracy of the retrieved result will be assessed by the complex error metric ε_{comp}.

A. Error Assessment and Influence of the Scan Radii

As an initial test, the two-scans technique is applied to an antenna defined by arranging the dipoles in a square array with uniform amplitude and phase excitation. The size of the array is $16\lambda \times 16\lambda$ (thus a truncation constant $N = 80$) and the angular oversampling $s = 2$. First, the set of distances $r_1 = 0.16r_{far}$ and $r_2 = 0.24r_{far}$ is selected. A second experiment is performed setting to $r_2 = 0.2r_{far}$. As already discussed in previous publications [20], [21], with an increasing separation between spheres, the amplitude fields

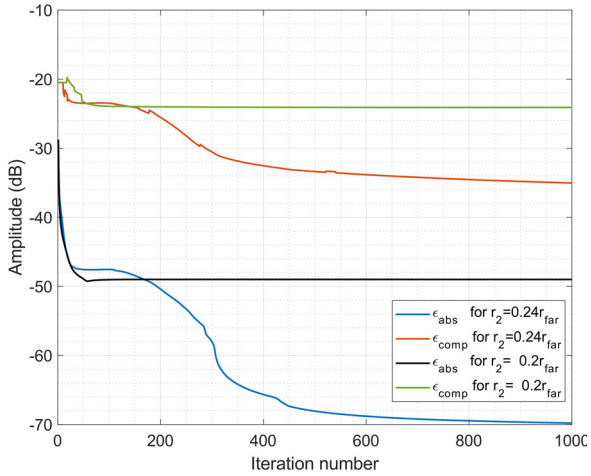

Fig. 1. Amplitude and complex error evolution for $r_1 = 0.16r_{far}$ and two different values of the second sphere radius.

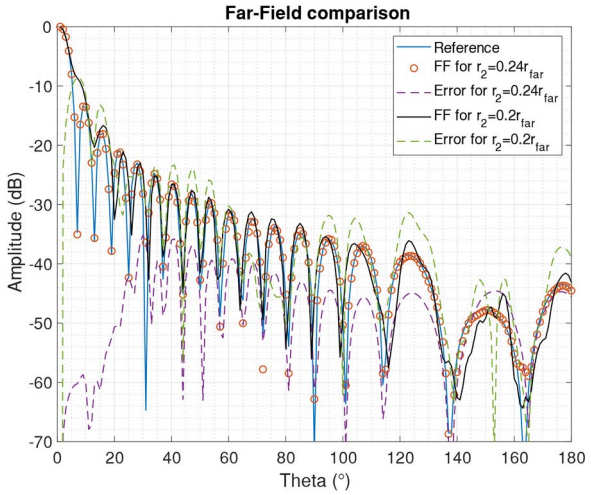

Fig. 2. Comparison of the retrieved radiation patterns from phaseless measurement using $r_1 = 0.16r_{far}$ and two different radii for the second sphere.

of the two surfaces become different, which improves the convergence of the algorithm to low error levels. This can be seen in Fig. 1 where the two introduced error metrics are depicted for each iteration of the algorithm. The amplitude error drops to -70 and -50 dB for the first and second experiments, respectively. However, this metric only gives a partial information because it does not consider the phase of the retrieved solution. When the SWC of the antenna are *a priori* known, as in this simulation example, the complex error can be calculated obtaining much higher values, -35 and -22 dB, respectively. The reason of the discrepancy between both error metrics is that there are at least two sets of SWC (i.e., with differences in the order of -35dB in the first simulation) which radiate relatively similar amplitude fields (differences of -70 dB) on the two measurement spheres.

The far-field of the retrieved coefficients for both experiments is calculated and compared with the true far-field of the AUT in Fig. 2. The error curves are computed by subtracting

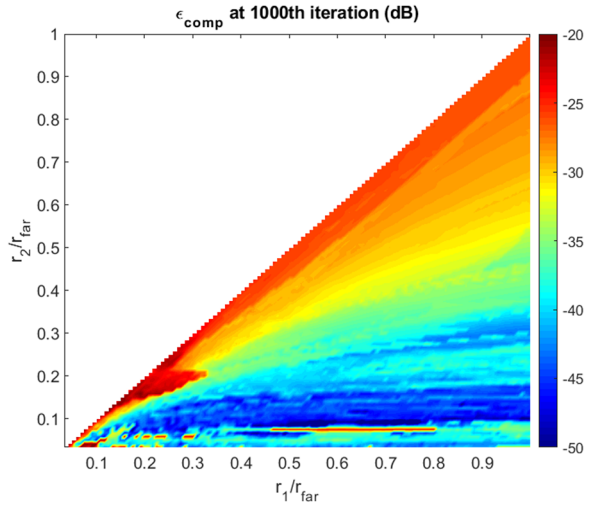

Fig. 3. Complex error map for each combination of normalized measurement radii for the AUT of size $N = 80$.

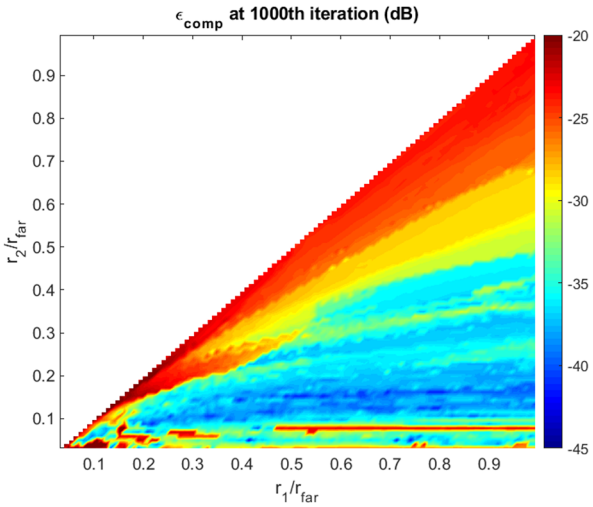

Fig. 4. Complex error map for each combination of normalized measurement radii for the AUT of size $N = 60$.

the complex far-fields. For the first experiment, this error goes as high as -35 dB. However, the amplitude values seem to be in closer agreement with the true far-field, even for values as low as -50 dB. The source of this discrepancy is due to the phase. A similar trend is observed for the second experiment but have higher error levels. In general, it has been observed that the phaseless technique retrieves better the amplitude than the phase values in the far-field, but this has not been thoroughly investigated. Note that this is not a trivial property as the far-field amplitude is influenced by both amplitude and phase in the near-field.

For better understanding of the influence of the measurement radius, both r_1 and r_2 are swept for different values, and the phaseless technique is applied for each combination. Fig. 3 depicts a 2-D plot of the complex error for the last iteration. From this figure some conclusions can be drawn. First, the optimum region for r_2 is around $0.1r_{far}$ and $0.15r_{far}$. In this region, even for small separations with respect to r_1 the retrieved coefficients show low errors. This may be due to the fact that, in that interval, the radiated amplitude fields experiment rapid variations with respect to the radial coordinate (this means higher differences between the two measured fields, thus more information). However, for values of r_2/r_{far} lower than 0.1 the error experiments abrupt increases for reasons not yet studied. Considering that the minimum sphere has a normalized radius of 0.01, any issue of AUT-probe colliding spheres is discarded.

B. Influence of AUT Size

The previous experiment is repeated reducing the array size so that its new truncation index is $N = 60$, obtaining an analogous 2-D error map depicted in Fig. 4. The obtained error distribution shows good agreement with the previous case, suggesting that the same trend may be extrapolated for other AUT sizes. This has been verified for $N = 40$ and 100 obtaining similar agreement. To further demonstrate this property, and additional test is conducted for $N = 120$ but fixing r_2/r_{far} to 0.5. Fig. 5 depicts the obtained errors for all simulated N values as a function of r_1/r_{far}. All curves for the different sizes show the same behavior confirming that the influence of the measurement radius is relative to the Rayleigh distance. The center of the plot (0.5) corresponds to the case where $r_1 = r_2$, so the error is the highest. When r_1 starts to differ, the error decreases, but not in a symmetric way: Setting r_1 closer to the antenna offers superior performance as we are approaching to the previously mentioned area with strongest variations with respect to the radial coordinate. Another noticeable issue is the irregular behavior of the curves showing ripples. This, along with the abrupt changes present in this figure and Figs. 3 and 4 are due to the non-linear nature of the phase retrieval algorithm, trapping it in suboptimal solutions which depend on the given measurement scenario. Finally, it is also observed that for bigger AUTs, the retrieved errors tend to be smaller. In general, electrically large AUT experiment a significant variation of the near-field amplitude with respect to the radial coordinate due to the high number of harmonics involved in the propagation. This has the effect of an increased diversity between the two measurement spheres leading to a better convergence.

C. Influence of AUT Type

Due to nonlinear nature of the phase retrieval problem, the previous results cannot be generalized to other antenna types without performing further experiments. The radiation characteristics over the two measurement spheres strongly depend on the specific AUT. This influence is investigated by simulating alternative AUT models typically encountered in near-field measurements scenarios. Six types of antennas will be simulated as follows.

1) A 20 dBi square planar array with a Taylor amplitude distribution with a sidelobe level (SLL) of -20 dB. In addition, a linear symmetric tapper up to 20° of phase is added along the columns.

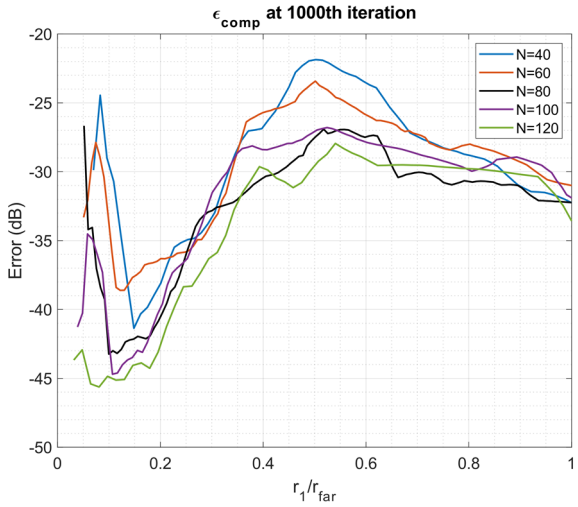

Fig. 5. Complex error for different values of r_1/r_{far} with a constant value of $r_2/r_{\text{far}} = 0.5$ for several AUT sizes.

2) A 32 dBi circular reflector antenna modeled as a 40λ radius aperture with an edge illumination of -10 dB and a circular blockage of 4λ.
3) A 25 dBi square planar array with uniform amplitude illumination and linear phase so the main beam is pointed to $\theta_p = 20°$.
4) The difference channel of a 2-D monopulse planar $10\lambda \times 10\lambda$ array. The monopulse is generated by dividing the aperture in four subarrays fed with 180° phase difference.
5) Three rectangular arrays of dimensions $15\lambda \times 7\lambda$, $15\lambda \times 5\lambda$ and $15\lambda \times 3\lambda$ with uniform excitation.
6) A linear array of printed dipoles with uniform excitation. The Huygens source is considered as a printed dipole.

The following test is conducted for the introduced antennas. Two spherical near-field measurements are simulated sweeping r_1 and fixing r_2/r_{far} to 0.5 and the angular oversampling is set to $s = 2$. Fig. 6 depicts the complex error after 1000 iterations of the phase retrieval algorithm. In the case of the square and circular arrays, the same behavior of Section III-B is observed. The monopulse difference pattern shows a significantly different performance, obtaining lager errors than the other types of antenna, especially for large values of r_1. The abrupt phase changes on the aperture may be the reason for the poor obtained results. Finally, the lower plot shows how the retrieved solution is degraded as the array aspect ratio changes in the rectangular arrays, reaching to the point that the algorithm gets trapped in a local minimum for all values of r_1 when the AUT is a linear array. The latter case has been re-simulated for all r_1 and r_2 combinations, without showing any significant improvement in the retrieved solution.

The conducted experiments show that the findings of Section III-A and III-B can be generalized for other AUT types with circular and square apertures with typical pencil beam patterns. For the case of linear and rectangular AUTs or special radiation patterns like monopulse, the phase retrieval degrades or even becomes totally unreliable, showing results difficult to generalize.

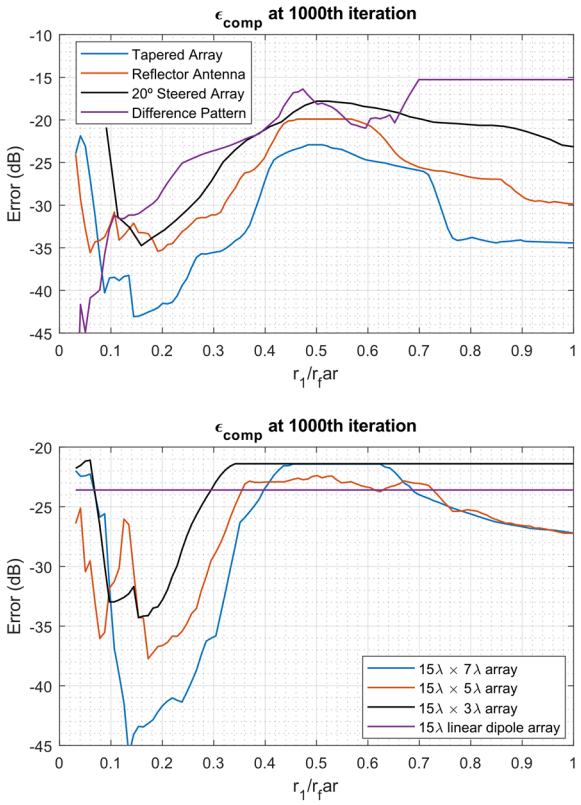

Fig. 6. Complex error for different values of r_1/r_{far} with a constant value of $r_2/r_{\text{far}} = 0.5$ for several AUT types.

D. Oversampling Assessment

In previous contributions, the effects of oversampling on phaseless techniques have been analyzed [9], [19], [22], proving to be a helpful or even mandatory tool to obtain a good level of convergence for the phase retrieval. The reason for this is that removing the phase from the field doubles its bandwidth. Therefore, experiments conducted so far have been performed with an angular oversampling of $s = 2$, which means that both angular increments (θ, φ) are divided by 2 with respect to the ones of a standard near-field measurement. This definition differs from the one used in other contributions [9] based on the number of degrees of freedom of the AUT radiated fields. Here we note that standard spherical near-field measurements usually acquire around twice as much samples as numbers of degrees of freedom of the AUT. Considering that we are measuring in two surfaces, in which the number of samples is doubled on each dimension, the total of samples amounts to roughly 16 times with respect to the number of degrees of freedom. This may seem an excessive number of measurement points and indeed becomes a drawback leading to long measurement times. However, even far higher values have been reported to improve other phaseless algorithms convergence [9].

The influence of this parameter is here analyzed for the spherical case using as AUT a $10\lambda \times 10\lambda$ square array with uniform amplitude and phase distribution. Several experiments are carried out sweeping the angular oversampling between 1 and 3.25 for different orientations keeping the sphere radii $r_1/r_{\text{far}} = 0.16$ and $r_2/r_{\text{far}} = 0.48$. The orientation is adjusted

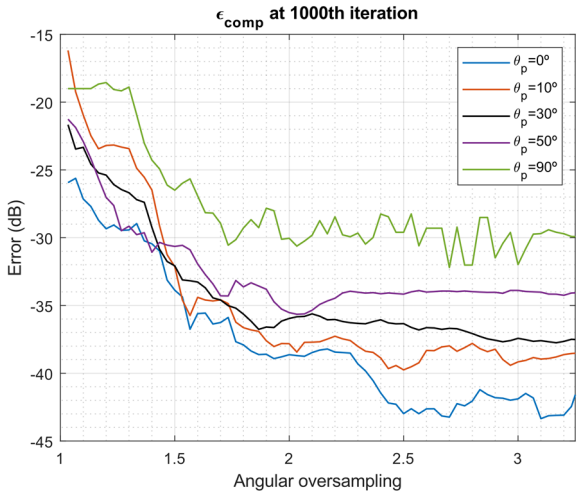

Fig. 7. Complex error as a function of the sampling rate for different AUT orientations.

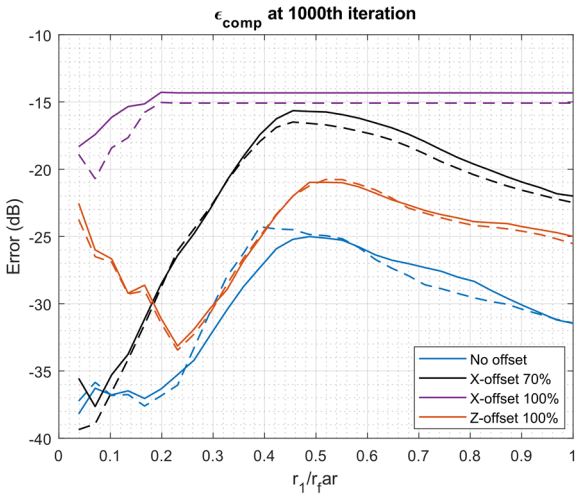

Fig. 8. Retrieved errors at different measurement distances for several AUT offsets using a Hertz dipole (continuous line) and 15 dBi antenna (dotted) as probes.

by rotating the antenna around the $\hat{x}$ axis so the main beam points to a given angle θ_p. This parameter is of significant relevance because the equiangular sampling commonly used in spherical near-field measurements samples more densely the poles than the equator. Depending on the antenna pointing, the near field will be better sampled in some regions than others, which may impact the phase retrieval process.

The retrieved errors are depicted in Fig. 7. Disregarding the irregular behavior characteristic of this technique, the main trend is a reduction of the error with increasing sampling rates. The error also increases as the antenna is rotated, which is an effect that cannot be compensated by adding more samples. We conclude that the loss in accuracy is not due to the main lobe becoming sparsely sampled. As in the previous section, a loss of AUT axial symmetry may be the reason for this degradation. In all cases, the minimum error tends to saturate for values higher than $s = 2$, so an angular oversampling around this value is welcomed for a more reliable phase retrieval.

E. Influence of Probe Directivity and AUT Offset

Single-order probe correcting capabilities are implicit in the proposed phase retrieval technique. All simulations performed so far have been obtained using an Hertzian dipole as ideal probe, so the measured signal is exactly the electric field in the probe location. Standard spherical measurements are performed usually with conical horns as probes with directivities ranging from 10 to 15 dBi. Depending on the measurement distance, the probe itself may influence significantly the measured signal. It is of interest to investigate its potential effects over the phase retrieval algorithm. This has already been studied for the planar case [15], showing how the probe influence can be exploited to perform phaseless measurements using two different probes instead of changing the measurement distance. It is well-known that the probe influence is far less significant in the spherical case; however, it is worth performing such analysis.

A square array of size $N = 80$ measured with angular oversampling $s = 2$ is simulated with $r_2/r_{\text{far}} = 0.5$ and sweeping r_1. The simulation is performed twice, one for a Hertzian dipole probe and the other for a 15 dBi antenna. The latter is obtained arranging several Hertz dipoles in a vertical array, as in a Yagi-Uda antenna, increasing its directivity while keeping its single-order nature. To further emphasize the probe effects, the AUT is simulated with different offset values with respect to the center of the measurement sphere. As a result, the probe "sees" the AUT from a different angle for every measurement point. This has also the effect of increasing the AUT minimum sphere, thus the truncation index and sampling rate are increased accordingly for the experiments. The offset values are denoted as percentages of the displacement from the center relative to the AUT diameter. The simulated offset values are: 70% and 100% in the $\hat{x}$ axis direction, and 100% in the $\hat{z}$ direction.

Fig. 8 depicts the retrieved errors from all the conducted experiments. For displacements along the $\hat{x}$ axis, the offset breaks the AUT axial symmetry, which degrades the performance of the algorithm. In the case of the $\hat{z}$ axis, the symmetry of the antenna is kept but the offset adds an additional phase variation to the measured near-field, which complicates the phase retrieval and also degrades the results but to a lesser extent. On the other hand, the probe shows no significant impact on the results, which makes it impossible to derive any relationship between the probe directivity and the algorithm convergence. This confirms that the influence of the probe has a small contribution which neither can be exploited nor can degrade the algorithm performance. For this experiment, a 15 dBi mono-mode probe has been selected as it is a typical on standard near-field measurements scenarios. Higher order probes with more complex radiation patterns may introduce a significant influence on the results. However, the phase retrieval technique employed here is not applicable in these cases.

F. Robustness Against Noise

Finally, the proposed technique is tested including noise to assess its robustness on real measurement scenarios. For this

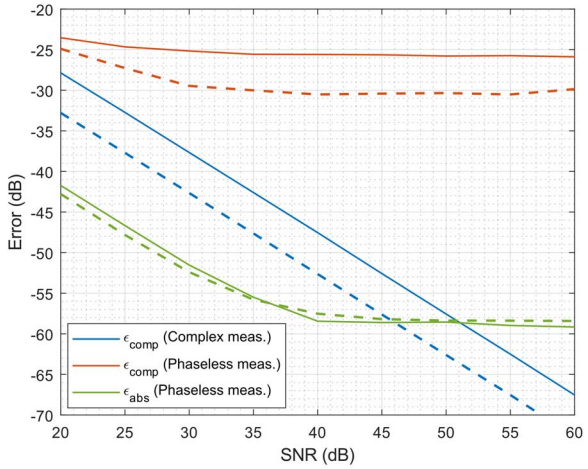

Fig. 9. Influence of the noise on the error of the retrieved solution for an angular oversampling s = 1.5 (continuous line) and s = 2.5 (dotted lines).

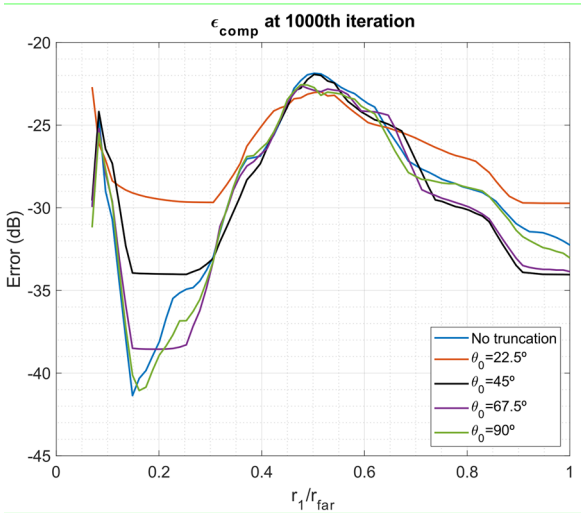

Fig. 10. Complex error for different values of r_1/r_{far} with a constant value of $r_2/r_{\text{far}} = 0.5$ for several polar truncation angles.

test we go back to the scenario of Section III-A with the AUT of size $N = 80$ with $r_1/r_{\text{far}} = 0.16$ and $r_2/r_{\text{far}} = 0.24$. For this configuration, complex additive white Gaussian noise is added to the measured signals before removing the phase. The phase retrieval technique is applied sweeping the signal-to-noise ratio (SNR) between 20 and 60 dB. This experiment has been repeated for two values of angular oversampling, $s = 1.5$ and $s = 2.5$. The retrieved errors have been depicted in Fig. 9 showing a high robustness even for poor SNR values. The complex error remains around the same value of the noise-free experiment for SNR values as high as 35 dB. Therefore, adding noise lower than this level will have little effect over the retrieved SWC. The effect over the amplitude error is more significant, but it also presents a good robustness achieving a saturation value around 40 dB of SNR. In addition, the complex measurements are processed to retrieve the SWC using traditional field transformation techniques [3] and ε_{comp} is computed for each SNR value as well. This is also depicted in Fig. 9 to compare the noise-filtering capabilities of both approaches.

Increasing the sampling rate has small effect on the noise robustness of phaseless measurements as compared with the complex case. In the phaseless case, the convergence values for ε_{abs} do not show a significant improvement. In the case of ε_{comp}, the obtained errors are lower, because increasing the sampling rate allows the phase retrieval algorithm fall in a local minimum closer to the optimal solution. The presence of noise then becomes a secondary issue, and a better SNR does not translate in lower errors as in the complex case. We conclude then that the proposed technique shows a well-conditioned response against noise, so for scenarios with good SNR values its effect will be negligible compared with the more problematic local minima issue.

G. Truncation of the Sphere

Truncated spherical measurements [32], [33] are common in scenarios where the full spherical surface cannot be acquired due to physical limitations, like in the case of automotive measurements. Alternatively, truncated acquisitions can be employed to reduce measurement times by just scanning the solid angle where most of the significant radiation is of interest. The most common case is the polar truncation, in which the near-field is only measured up to a given $\theta = \theta_0$. This has the effect of limiting the retrieval of the transformed far-field up to a given reliable angle slightly smaller than θ_0 [3].

The truncation effects are investigated here for phaseless spherical near-field measurements. The same test of Fig. 5 is conducted again for the array of size $N = 40$, but this time, the input field on the two spheres is truncated to several values θ_0. Fig. 10 depicts the evolution of the different complex errors as a function of the first sphere radii. For moderate levels of truncation, its effects are negligible in comparison to the inherent errors of the phase retrieval process. When a significant part of the near-field power is truncated, the accuracy of the phase retrieval is reduced in those radial regions where the separation between spheres was high enough. This loss in accuracy is proportional to the truncation value in a stable way, which suggests that the phase retrieval is well conditioned against truncation errors in a similar way as conventional complex measurements.

The truncation effect has also been evaluated in the far-field. Fig. 11 depicts the retrieved far-field from the phaseless experiment for $r_1/r_{\text{far}} = 0.2$, which is around the optimal performance region. The true analytical far-field has been depicted too. It can be observed that the different patterns show perfect agreement with the reference for smaller angles than θ_0.

H. Antenna Parameters Assessment

The error metric ε_{comp} gives an overall description of the accuracy of the retrieved solution but its relationship with the quality of the reconstructed radiation pattern is not straightforward. Antenna parameters such as directivity, beamwidth (BW), and SLL are of high interest because they

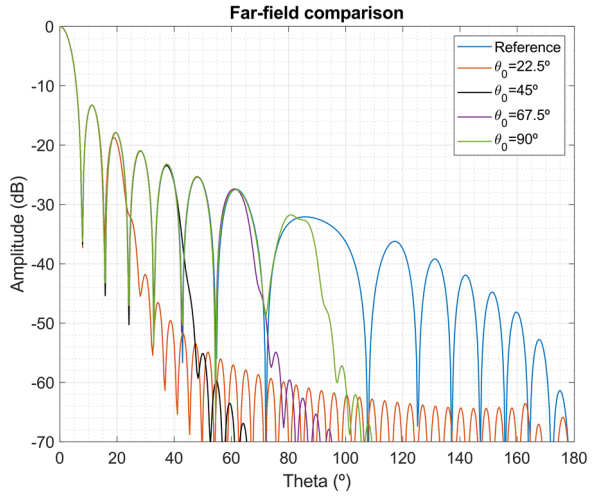

Fig. 11. Transformed far-field from several polar truncated acquisitions along with the reference far-field for $r_1/r_{\text{far}} = 0.2$ and $r_2/r_{\text{far}} = 0.5$.

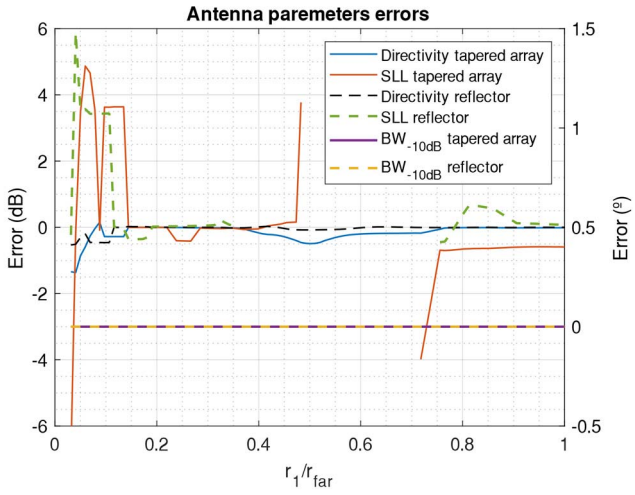

Fig. 12. Evolution of antenna parameters for different values of r_1/r_{far} with a constant value of $r_2/r_{\text{far}} = 0.5$ for several AUT types.

directly affect the performance of the antenna application. Therefore, it is worth performing a specific analysis on the quality of these parameters obtained from the phase retrieval algorithm.

The experiments performed on Section III-C are repeated here for the tapered array and reflector antennas. For each simulation, the directivity, first SLL, and -10 dB BW are calculated. The errors of these parameters with respect to the reference solution are computed and depicted in Fig. 12, in the same way as Fig. 6. It is noticeable that the algorithm can retrieve the -10 dB BW with perfect accuracy in all cases, even for the region where the spheres are too close resulting in high ε_{comp} values. The directivity value is mostly influenced by the main lobe, so it is retrieved with good accuracy in all cases too. The first SLL constitutes a more challenging parameter to retrieve, as both antennas are designed for a level around -20 dB. For both antennas, the SLL curves show an empty region where the error is not shown. This corresponds to the region with high ε_{comp} values, where the retrieved patterns where so distorted that the SLL calculation was giving meaningless results.

I. Guidelines for Phaseless Spherical Measurements

From the analysis performed in the previous subsections, it becomes evident that the two-scans phaseless technique requires a careful choosing of some parameters in order to obtain a successful near-field to far-field transformation. As a summary, the main conclusions are summarized here to give a set of guidelines to consider when performing such type of measurements in real anechoic chambers.

1) The spherical phaseless retrieval method is an ill-posed technique prone to problematic behavior. Convergence to acceptable error levels is not guaranteed for an arbitrary antenna, so the specific AUT type must be considered carefully.
2) AUTs with good axial symmetry around $\hat{z}$ and pencil beam patterns are the best candidates for accurate phaseless measurements. Beam steered and rectangular aperture antennas with some level of symmetry show good convergence capabilities too. On the other hand, linear arrays or specific antennas with unconventional radiation patterns, poor symmetries, high aspect ratios, significant offsets with respect to the minimun sphere, or abrupt aperture phase changes become problematic or even impossible to process with the introduced technique.
3) Relative separation between spheres is a critical parameter, but the absolute radii are also relevant. The best results are obtained with the smallest sphere having a radius of 10%–15% of the Rayleigh distance, and at least 20%–30% respectively for the second sphere.
4) Some degree of angular oversampling, ideally around 200% with respect to standard spherical measurements, significantly reduces the retrieved errors.
5) Probe correction, polar truncation and thermal noise play a minor role on the accuracy of the retrieved solution if they remain on the margins of standard spherical near-field measurements.
6) The use of an initial guess improves the algorithm convergence. This has already been shown in previous publications [20], [21], so it has not been repeated here. The investigations performed in this article are intended to be generic without need of any prior information about the AUT. Therefore, the initial guess used in this study uses only the polarization type information about the AUT, so it has a small influence. Some of the previous tests have been repeated without such guess obtaining slightly worse convergence levels.

The limitations imposed by the used iterative Fourier algorithm should be considered too. Because the alternating projections between the two spheres are performed using a classical near-field transformation approach, the introduced technique shares the same limitations. Measurements are restricted to single-order probes and equiangular sampling, so it is not possible to take advantage of the benefits provided by higher order probes [33] and nonuniform sampling [34]. This could be solved by use of modern techniques, but they are less

computationally efficient, and the implementation of the algorithm becomes more complex.

Finally, the two-scans phaseless technique can be addressed by use of alternative phase retrieval algorithms. During the last years, multiple techniques [10] have been proposed that could be implemented in the spherical case. An interesting feature of such techniques is the incorporation of initializers which estimate a good starting point for the iterative process to alleviate local minima issues. This could improve the convergence values of the introduced method, especially in the cases of antennas with complicated radiation patterns. The implementation of these techniques requires the use of matrix formulation following a different approach than the one presented in this article, which can lead to a more complex and computationally demanding alternative.

IV. Anechoic Chamber Phaseless Measurements

Finally, the two-scans spherical phaseless near-field to far-field transformation technique is tested using measured data. Some preliminary measurements done at the DTU-ESA facility were discussed in [21]. In that measurement campaign, physical limitations of the positioner equipment inhibited the use of adequate separation between spheres, so the more relevant examples were done using partially synthetic data. In this section, however, pure measured data will be used obtaining positive results. This time the measurements have been performed in the anechoic chamber of the Technical University of Madrid (UPM). The used spherical range consists in a roll-over-azimuth positioner with a translation stage so that spherical measurements can be performed with radii ranging between 3 and 5.5 m. Two different antennas will be tested, a 20 GHz parabolic reflector and the mmVAST at 37.8 GHz.

A. 20 GHz Reflector Antenna

The first antenna to be tested is a 20 GHz reflector antenna of 60 cm diameter with linear polarization and around 40 dBi of gain. According to its electrical dimensions, the truncation index for this AUT has a value of $N = 120$ whereas the far-field distance is around 38 m. Two spherical measurements at 3 and 5.5 m of distance are performed so that the complete range of movement of the translation stage is exploited. These radii correspond to the 8% and 15% of the Rayleigh distance respectively, which is somewhat close to the optimal range according to the previously derived criteria. The spherical measurements are performed with angular increments of 1° so that an angular oversampling of 1.5 is obtained. The probe consists of a smooth-walled conical horn with axial corrugations and 15 dBi of directivity, which is rotated 90° on each measurement point to measure both field polarizations.

Both spherical near-field measurements are performed recording amplitude and phase of the received signals on the probe. From the complex measurement at 5.5 m, the far-field and the SWC are computed using the commercial software SNIFT [35]. The SWC are used to perform near-field simulations at arbitrary measurement distances. Multiple combinations of r_1 and r_2 are used to simulate virtual measurements of the AUT with the same probe and angular sampling. For each

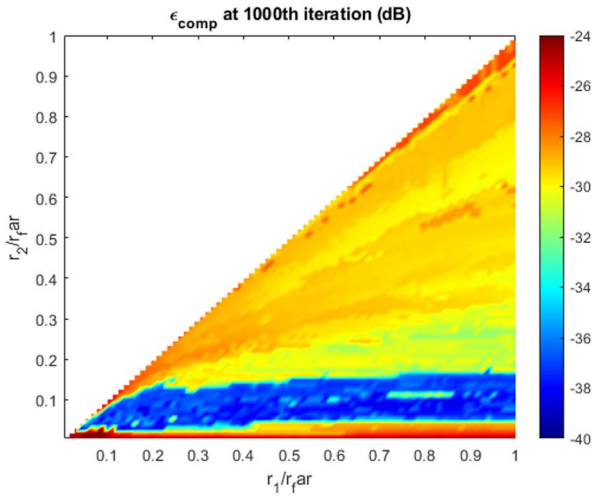

Fig. 13. Complex error map for each combination of normalized measurement radii for the measured 20 GHz reflector antenna.

(r_1, r_2) pair, the phase retrieval technique is applied using the amplitude of the simulated fields. The obtained convergence values are depicted in Fig. 13, where nice agreement with the analytical simulations is observed. It can be confirmed that the selected measurement distances lie in the region of optimal performance, although with little margin. This becomes possible for this particular AUT and measurement range, but for other frequencies and antenna dimensions, the required measurement radii for an optimal performance may be unfeasible due to mechanical limitations.

Now, the two-scans phaseless technique is applied using the amplitude information of the two pure measurements without any prior postprocessing. The algorithm is evaluated for 1000 iterations using as initial guess an Hertzian dipole with the same polarization as the AUT. Fig. 14 depicts a comparison between the complex far-field processed by SNIFT and the one obtained using the phaseless iterative algorithm. A point-by-point far-field error metric is given by the equivalent error signal (EES), as specified by

$$EES(\theta,\varphi) = 20log_{10}\left(\frac{\left|\left|E(\theta,\varphi)_{comp}\right| - \left|E(\theta,\varphi)_{ph}\right|\right|}{max\left(\left|E(\theta,\varphi)_{comp}\right|\right)}\right) \quad (5)$$

being $E(\theta,\varphi)_{comp}$ and $E(\theta,\varphi)_{ph}$ the far-field patterns retrieved from the complex and phaseless data, respectively. Good agreement is exhibited by the co-polar pattern, yet the cross-polar EES is relatively high.

In addition, the same process is repeated but instead of using the pure amplitude measurements, the simulated amplitudes obtained from the SWC in the same spheres are used. This showcases the effect of the different sources of errors affecting both measurement spheres independently. The corresponding radiation pattern and EES are depicted in Fig. 14 as well, and it can be appreciated how the use of postprocessing to generate the fields on the two spheres gives a result with significantly lower errors. When pure phaseless measurements are considered, amplitude drifts, spurious reflections, and mechanical misalignments between the two measurement surfaces lead to degradation. Yet these are normal sources of uncertainties

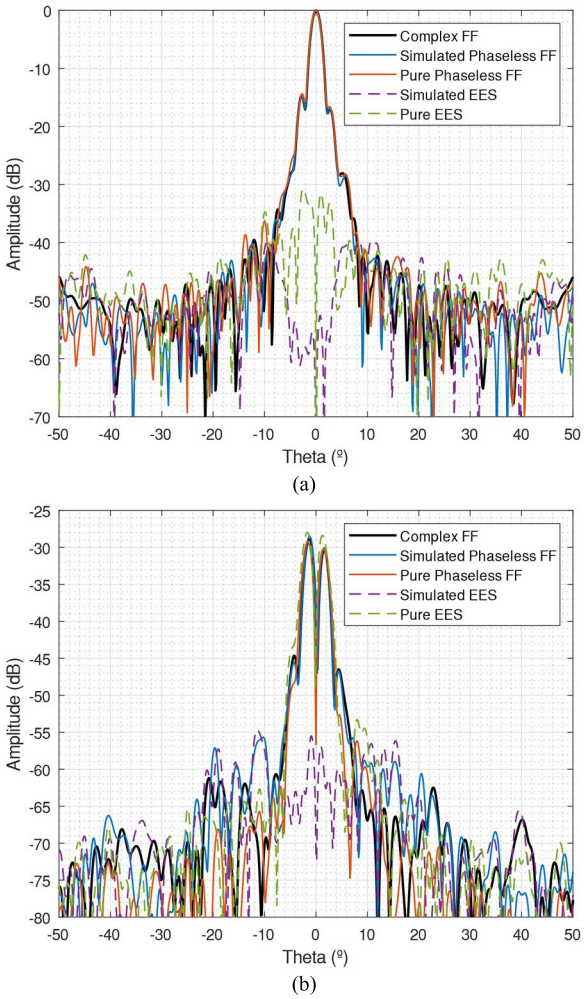

Fig. 14. Transformed far-field of the 20 GHz reflector antenna: (a) co-polar and (b) cross-polar components.

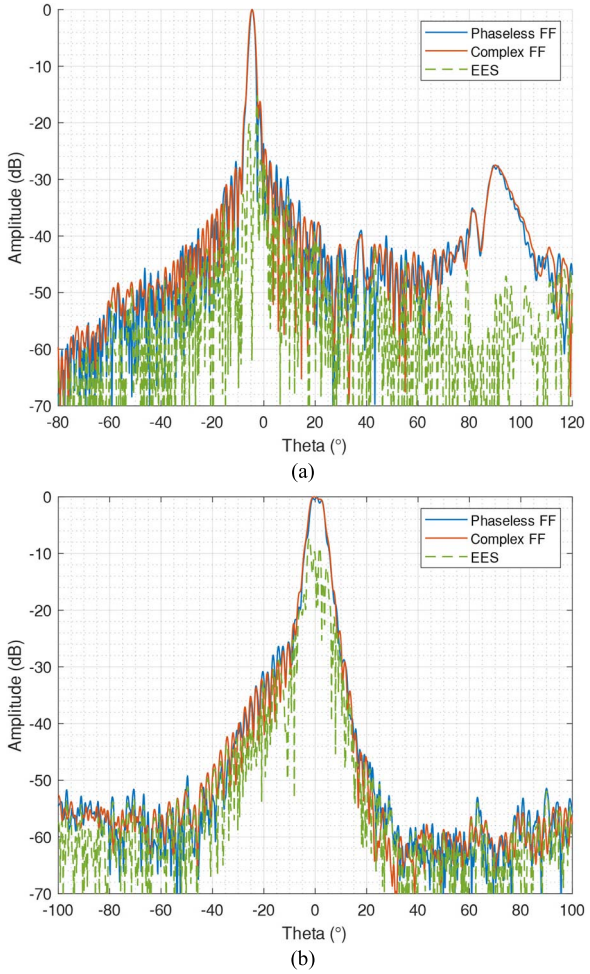

Fig. 15. Transformed far-field of the mmVAST antenna for the (a) E- and (b) H-planes. Coordinate rotations have been applied to align the H cut with the main beam.

in standard complex measurements one should expect an increased robustness for amplitude-only measurements. However, the ill-condition nature of the phaseless problem can amplify these errors compromising its reliability.

B. mmVAST 40 GHz Measurements

The DTU-ESA millimeter-wave validation standard antenna (mmVAST) [36] is an offset single-reflector antenna with an astigmatic paraboloid having different focal lengths in the orthogonal offset and transverse planes. This asymmetry gives rise to different beam widths in these planes and thus a non-circular misaligned main beam, which becomes a challenging pattern to measure. The antenna has an aperture dimension of 230 mm $\times$ 230 mm with an enclosing box of 530 mm $\times$ 230 mm $\times$ 440 mm. The reflector is fed by a cluster of four Pickett-Potter horns, one for each of the four operational frequencies (19.76, 30.04, 37.80, and 48.16 GHz).

For this test, the 37.8 GHz frequency is selected with circular polarization. Considering its electrical dimensions at the selected frequency, the truncation index for the mmVAST is $N = 250$ and its Rayleigh distance 91 m. Once again, the measurement radii are set to 3 and 5.5 m but in this case, they correspond to a 3.3% and 6% of the far-field distance. These are very low values, far from the optimal region derived in the previous section, but the best ones that can be obtained due to the mechanical limitations. This means that the two spheres are not separated enough, and all propagating spherical waves cannot experiment the required variations to ensure a good convergence of the phaseless technique. However, it is interesting to study the behavior of the technique under such circumstances, especially for a challenging antenna like the mmVAST. The measurements are also done with two orthogonal orientations of a similar probe, and angular increments of 0.5° are selected providing an angular oversampling ratio of 1.44.

As in the previous case, two complex measurements are performed, and the reference far-field pattern is obtained from the largest sphere. Then the two-scans spherical phaseless technique is applied using the amplitude information of both measurements using as initial guess two crossed Hertz dipoles generating circular polarization. Fig. 15 depicts the obtained radiation pattern along with the reference solution for the two principal cuts, which have been obtained by means of coordinate system rotations, due to the AUT off-axis beam pointing direction. In addition, the far-field pattern for the

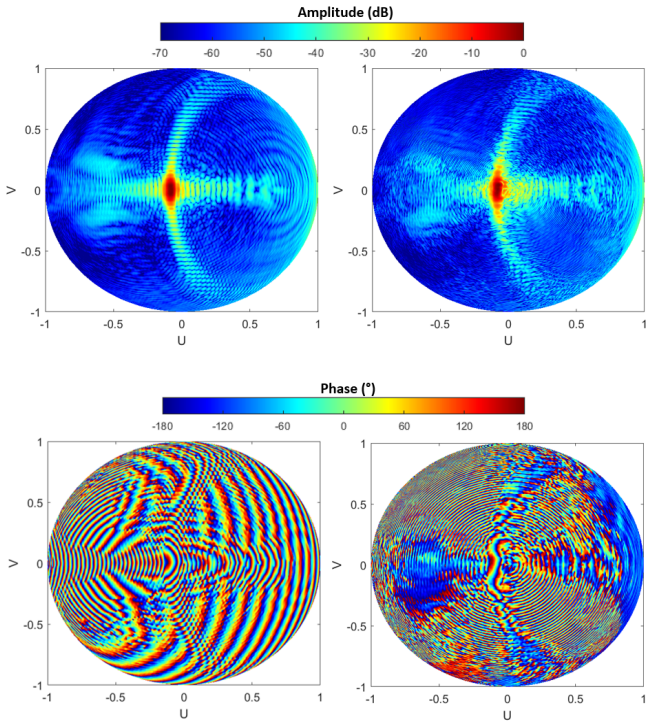

Fig. 16. Amplitude and phase UV plots of the (left) complex and (right) phaseless far-field $\hat{\theta}$-component patterns for the mmVAST antenna.

forward hemisphere in UV coordinates has been depicted in Fig. 16. The agreement is not as good as in the previous case, but the main lobe is well retrieved and there is a high similarity in the secondary far-lobes.

Unlike in the previous case, the far-field cuts are plotted only in magnitude and not by co and cross-polar components. The reason for this is that the algorithm is not able to retrieve properly the phase of both $\hat{\theta}$ and $\hat{\varphi}$ components, which is critical to correctly generate the circular polarization components. Fig. 16 depicts the phase of the far-field $\hat{\theta}$ component for both complex and phaseless cases. There is not agreement whatsoever between both plots so it can be concluded that the algorithm is unable to retrieve the phase for this antenna.

V. Conclusion

The two-scans phaseless spherical near-field measurement technique has been reviewed and thoroughly investigated. The lack of phase must be compensated with amplitude measurements adding enough "field information" so the algorithm can reach a good level of convergence. Such additional information is generated by separating the spheres well enough. It has been shown how this separation is relative to the Rayleigh distance of the corresponding AUT, and certain combinations of sphere radii tend to provide the best results. In addition, the influence of the AUT has been studied, showing how the technique provides better results for centered antennas with good axial symmetry. In the case of linear arrays or complicated radiation patterns, the technique becomes unreliable. It has been confirmed that the use of oversampling with respect to conventional complex measurements helps to improve the accuracy of the algorithm. The robustness of the technique with respect to noise, polar truncation, and probe influence has been demonstrated as well. Finally, the previous observations have been considered to perform pure near-field phaseless measurements in the Technical University of Madrid of two different antennas, obtaining results in agreement with the conducted numerical studies.

Future work includes the study of alternative phase retrieval methods with different initializers, to assess its influence on the convergence values and processing times. The effect of the expansion basis for the problem will be also investigated. Some contributions follow approaches based on equivalent currents which can give additional information about the AUT structure, but they can lead to worse conditioned problems.

Acknowledgment

The authors thank Cristian Martínez Portas and Xiaoliang Sun for performing the antenna measurements of Section IV.

References

[1] *IEEE Recommended Practice for Near-Field Antenna Measurements*, IEEE Standard 1720-2012, Dec. 5, 2012, pp. 1–102.
[2] *IEEE Standard Test Procedures for Antennas*, ANSI/IEEE Standard 149-1979, 1979, p. 1.
[3] J. E. Hansen, *Spherical Near-Field Antenna Measurements*. London, U.K.: Peter Peregrinus, 1988.
[4] O. Breinbjerg and F. A. Javier, "Phaseless near-field antenna measurement techniques—An overview," in *Proc. 38th Annu. Symp. Antenna Meas. Techn. Assoc.*, 2016, pp. 314–319.
[5] M. D. Migliore and G. Panariello, "A comparison of interferometric methods applied to array diagnosis from near-field data," *IEE Proc.-Microw., Antennas Propag.*, vol. 148, no. 4, pp. 261–267, Aug. 2001.
[6] S. Costanzo, G. Di Massa, and M. D. Migliore, "A novel hybrid approach for far-field characterization from near-field amplitude-only measurements on arbitrary scanning surfaces," *IEEE Trans. Antennas Propag.*, vol. 53, no. 6, pp. 1866–1874, Jun. 2005.
[7] J. L. Martinez, A. Arboleya-Arboleya, Y. Alvarez-Lopez, C. Garcia-Gonzalez, and F. Las-Heras, "Phaseless antenna diagnostics based on off-axis holography with synthetic reference wave," *IEEE Antennas Wireless Propag. Lett.*, vol. 13, pp. 43–46, 2014.
[8] O. M. Bucci, G. D'Elia, G. Leone, and R. Pierri, "Far-field pattern determination from the near-field amplitude on two surfaces," *IEEE Trans. Antennas Propag.*, vol. 38, no. 11, pp. 1772–1779, Nov. 1990.
[9] A. Paulus, J. Knapp, and T. F. Eibert, "Phaseless near-field far-field transformation utilizing combinations of probe signals," *IEEE Trans. Antennas Propag.*, vol. 65, no. 10, pp. 5492–5502, Oct. 2017.
[10] R. Chandra, Z. Zhong, J. Hontz, V. McCulloch, C. Studer, and T. Goldstein, "PhasePack: A phase retrieval library," in *Proc. 51st Asilomar Conf. Signals, Syst., Comput.*, Oct. 2017, pp. 1617–1621.
[11] R. Pierri and R. Moretta, "On the sampling of the fresnel field intensity over a full angular sector," *Electronics*, vol. 10, no. 7, p. 832, Mar. 2021.
[12] F. R. Varela, B. G. Iraguen, M. S. Castaner, J. F. Alvarez, M. Mattes, and O. Breinbjerg, "Combination of spherical and planar scanning for phaseless near-field antenna measurements," in *Proc. Antenna Meas. Techn. Assoc. Symp. (AMTA)*, San Diego, CA, USA, Oct. 2019, pp. 1–6.
[13] R. T. Sánchez, F. R. Varela, L. J. Foged, and M. S. Castañer, "Reconstruction of relative phase of self-transmitting devices by using multi-probe solutions and non-convex optimization," *Sensors*, vol. 21, no. 7, p. 2459, Apr. 2021.
[14] A. Paulus and T. F. Eibert, "Exploiting spatial derivative information in phaseless near-field far-field transformations," in *Proc. 14th Eur. Conf. Antennas Propag. (EuCAP)*, Copenhagen, Denmark, Mar. 2020, pp. 1–5.
[15] R. Pierri, G. D'Elia, and F. Soldovieri, "A two probes scanning phaseless near-field far-field transformation technique," *IEEE Trans. Antennas Propag.*, vol. 47, no. 5, pp. 792–802, May 1999.
[16] R. G. Yaccarino and Y. Rahmat-Samii, "Phaseless bi-polar planar near-field measurements and diagnostics of array antennas," *IEEE Trans. Antennas Propag.*, vol. 47, no. 3, pp. 574–583, Mar. 1999.
[17] S. Razavi and Y. Rahmat-Samii, "A new look at phaseless planar near-field measurements: Limitations, simulations, measurements, and a hybrid solution," *IEEE Antennas Propag. Mag.*, vol. 49, no. 2, pp. 170–178, Apr. 2007.

[18] J. F. Alvarez, S. Pivnenko, and O. Breinbjerg, "Probe-corrected phaseless planar near-field antenna measurements at 60 GHz," in *Proc. 37th Annu. Symp. Antenna Meas. Techn. Assoc.*, 2015, pp. 314–319.
[19] J. F. Alvarez and O. Breinbjerg, "A computational and experimental investigation of $\lambda/2$ and $\lambda/4$ sampling step in phaseless planar near-field measurements at 60 GHz," in *Proc. 12th Eur. Conf. Antennas Propag. (EuCAP)*, London, U.K., 2018, pp. 1–5.
[20] C. H. Schmidt, S. F. Razavi, T. F. Eibert, and Y. Rahmat-Samii, "Phaseless spherical near-field antenna measurements for low and medium gain antennas," *Adv. Radio Sci.*, vol. 8, pp. 43–48, Sep. 2010.
[21] J. F. Alvarez, J. M. Bjørstorp, and O. Breinbjerg, "Spherical phaseless probe-corrected near-field measurements of the DTU-ESA VAST12 reflector antenna," in *Proc. 40th Annu. Symp. Antenna Meas. Techn. Assoc.*, 2018, pp. 216–221.
[22] A. Bangun, C. Culotta-López, A. Behboodi, R. Mathar, and D. Heberling, "On phaseless spherical near-field antenna measurements," in *Proc. 13th Eur. Conf. Antennas Propag. (EuCAP)*, Krakow, Poland, 2019, pp. 1–5.
[23] T. B. Hansen and A. D. Yaghjian, *Plane-Wave Theory of Time-Domain Fields: Near-Field Scanning Applications*. Hoboken, NJ, USA: Wiley, 1999.
[24] Y. Alvarez, F. Las-Heras, and M. R. Pino, "The sources reconstruction method for amplitude-only field measurements," *IEEE Trans. Antennas Propag.*, vol. 58, no. 8, pp. 2776–2781, Aug. 2010.
[25] B. Fuchs, M. Mattes, S. Rondineau, and L. L. Coq, "Phaseless near-field antenna measurements from two surface scans—Numerical and experimental investigations," *IEEE Trans. Antennas Propag.*, vol. 68, no. 3, pp. 2315–2322, Mar. 2020.
[26] M. García-Fernández *et al.*, "Antenna diagnostics and characterization using unmanned aerial vehicles," *IEEE Access*, vol. 5, pp. 23563–23575, 2017.
[27] F. Jensen and A. Frandsen, "On the number of modes in spherical wave expansion," in *Proc. 26th Annu. Symp. Antenna Meas. Techn. Assoc.*, 2004, pp. 489–494.
[28] J. R. Fienup, "Phase retrieval algorithms: A comparison," *Appl. Opt.*, vol. 21, no. 15, pp. 2758–2769, Aug. 1982.
[29] R. W. Gerchberg, "A practical algorithm for the determination of phase from image and diffraction plane pictures," *Optik*, vol. 35, no. 2, pp. 237–246, 1972.
[30] C. H. Schmidt, D. T. Schobert, and T. F. Eibert, "Electric dipole based synthetic data generation for probe-corrected near-field antenna measurements," in *Proc. 5th Eur. Conf. Antennas Propag. (EUCAP)*, Rome, Italy, 2011, pp. 3269–3273.
[31] L. J. Foged, L. Duchesne, P. Garreau, P. O. Iversen, and J. C. Bolomey, "Truncation impact on measured radiation pattern in spherical near field antenna test ranges," in *Proc. IEEE APS Symp. USNC-URSI Nat. Radio Sci. Meeting*, Jul. 2001.
[32] R. C. Wittmann, C. F. Stubenrauch, and M. H. Francis, "Spherical scanning measurements using truncated data sets," in *Proc. 24th Annu. Symp. Antenna Meas. Techn. Assoc.*, 2002, pp. 279–283.
[33] T. Laitinen, S. Pivnenko, J. M. Nielsen, and O. Breinbjerg, "Theory and practice of the FFT/Matrix inversion technique for probe-corrected spherical near-field antenna measurements with high-order probes," *IEEE Trans. Antennas Propag.*, vol. 58, no. 8, pp. 2623–2631, Aug. 2010.
[34] R. Cornelius, *Fast Spherical Near-Field Antenna Measurement Methods*. Aachen, Germany: Apprimus Verlag, 2019.
[35] *SNIFT Software*, TICRA, Copenhagen, Denmark, 2021. [Online]. Available: http://www.ticra.com
[36] O. S. Kim *et al.*, "DTU-ESA millimeter-wave VAlidation STandard antenna (mm-VAST)-detailed design," in *Proc. 9th Eur. Conf. Antennas Propag. (EUCAP)*, Lisbon, Portugal, 2015, pp. 1–4.

Fernando Rodríguez Varela was born in Ourense, Spain, in 1994. He received the M.Sc. degree in telecommunication engineering from the Technical University of Madrid, Madrid, Spain, in 2018, where he is currently pursuing the Ph.D. degree in near-field to far-field transformation techniques.

His current research interests include antenna design and antenna measurement and postprocessing techniques.

Javier Fernandez Álvarez was born in Gijón, Spain, in 1990. He received the degree in telecommunications engineering from the University of Oviedo, Oviedo, Spain, in 2015. He is currently pursuing the Ph.D. degree in phaseless near-field measurements with the Technical University of Denmark, Kongens Lyngby, Denmark.

He has been a Research Assistant with the Technical University of Denmark (DTU) since 2015. His research interests lay in the fields of antenna measurements and processing techniques.

Belén Galocha Iragüen was born in Bretoña (Lugo), Spain, in 1964. She received the degree in telecommunication engineering and the Ph.D. degree from the Technical University of Madrid (UPM), Madrid, Spain, in 1988 and 1992, respectively.

Since 1992, she has been with the Radiation Group of Signals, Systems and Radio-Communications Department, UPM, as an Associate Professor. Her current research interests include horn antennas, aperture antennas, and microwave passive devices.

Manuel Sierra Castañer (Senior Member, IEEE) was born in Zaragoza, Spain, in 1970. He received the degree in telecommunication engineering and the Ph.D. degree from the Technical University of Madrid (UPM), Madrid, Spain, in 1994 and 2000, respectively.

He worked for the Cellular Company Airtel, Madrid, from 1995 to 1997. Since 1997, he worked with the University Alfonso X, Madrid, as an Assistant, and since 1998 with the Technical University of Madrid, as a Research Assistant, an Assistant Professor, an Associate Professor, and finally a Senior Professor since 2017. He has been a Visitor Researcher with Tokyo Tech, Tokyo, Japan, (September–December 1998) and EPFL, Laussane, Switzerland, (September–December 1999) during his Ph.D. and a Visitor Professor with Tokyo Tech during the summers of 2012 and 2013. His current research interests are in planar antennas and antenna measurement systems.

Dr. Sierra-Castañer is a fellow of AMTA Society. Since January 2016 he has been a member of the EurAAP Board of Directors, where he is currently a Vice-Chair. He is the Director of the UPM Telecommunication Engineering School since May 2021. He obtained the IEEE APS 2007 Schelkunoff Prize Paper Award for the Paper Dual-Polarization Dual-Coverage Reflectarray for Space Applications in 2007 and other awards for papers in conferences. He has been AMTA Europe Liaison since 2015 until end of 2019.

Olav Breinbjerg (Fellow, IEEE) was born in Silkeborg, Denmark, in 1961. He received the M.Sc. and Ph.D. degrees in electrical engineering from the Technical University of Denmark (DTU), Kongens Lyngby, Denmark, in 1987 and 1992, respectively.

He was with the Faculty of the Department of Electrical Engineering, as an Assistant Professor from 1991 to 1995, an Associate Professor from 1995 to 2005, and a Full Professor from 2006 to 2021. From 1997 to 2021, he was also the Head of the Electromagnetic Systems Group and the DTU-ESA Spherical Near-Field Antenna Test Facility. He resigned his position with DTU in May 2021. He is currently an Independent Consultant. He was a Visiting Scientist with the Rome Laboratory, Rome, NY, USA, in 1988, a Fulbright Research Scholar with the University of Texas at Austin, Austin, TX, USA, in 1995, and a Visiting Professor with the University of Sienna, Siena, Italy, in 2011. He has been the Main Supervisor of 17 Ph.D. students. He is the author or coauthor of more than 60 journal articles, 200 conference articles, and 150 technical reports. His research is generally in applied electromagnetics—and particularly in antennas, antenna measurements, computational techniques, and scattering—for applications in wireless communication and sensing technologies.

Dr. Breinbjerg is a fellow of AMTA. He was a recipient of the U.S. Fulbright Research Award in 1995, the 2001 AEG Elektron Foundation's Award, the 2003 DTU Student Union's Teacher of the Year Award, the 2013 and 2015 European School of Antennas Teacher of the Year Awards, and the 2020 Hans Christian Ørsted Award.